Improved Ferrite Number Prediction Model that Accounts for Cooling Rate Effects – Part 2: Model Results

Results of a prediction model based on a neural network system of analysis are described

BY J. M. VITEK, S. A. DAVID, AND C. R. HINMAN

ABSTRACT. A new Ferrite Number prediction model, ORFN (Oak Ridge Ferrite Number), was developed in Part 1 of this study (*Welding Journal*, January 2003) and, in this contribution, the model predictions are evaluated and compared with predictions of other models. The ORFN quantitatively takes account of cooling rate effects on the Ferrite Number for the first time. It is shown the new ORFN model presents very good agreement with experimental data and is significantly more accurate than existing constitution diagrams or recently developed composition-only neural network models. The model is equally valid for austenitic stainless steels and duplex stainless steels. Furthermore, the model is applicable to both conventional arc welding conditions as well as high cooling rate conditions prevalent during high energy beam welding, such as laser beam welding, and high-speed arc welding.

Introduction

Stainless steel welds typically contain a two-phase microstructure with anywhere from a few percent to more than 50% ferrite in an austenite matrix. Numerous models have been proposed over the years to predict ferrite content (or Ferrite Number[1]) in stainless steel welds (Refs. 2–12; see Ref. 6 for a review of earlier models). In all these models, the predicted ferrite content is based on the alloy composition alone. This applies for both traditional constitution diagrams as well as more recently developed models, including neural network models. However, it is well known cooling rate can have a significant effect on the Ferrite Number (FN), especially for laser beam welds, high-speed arc welds, and duplex stainless steel welds. In Part 1 of this paper, the basis for the cooling rate effect was reviewed and the need for a better predictive model outlined (Ref. 13). Also in Part 1, the details and procedures for developing an improved predictive model that includes cooling rate were described, including the generation of the dataset required for the new model development. In this portion of the two-part study, after a very brief overview of some of the features of the dataset generation and model development, the results of the model are presented. The predictability of the new Oak Ridge Ferrite Number (ORFN) model, which includes consideration of cooling rate, is evaluated and the model results are compared with existing composition-only models.

Model Development

The new ORFN model is based on a neural network analysis. This type of analysis is nonlinear in nature and thereby allows for identification of complex elemental interaction effects missed in more traditional models based on a regression analysis. It was shown in earlier neural network models based only on alloy composition that the predictions were significantly more accurate than those using other approaches (Refs. 10–12). The optimum neural network architecture for ORFN was identified by a procedure described in Refs. 10 and 13. Using this optimum architecture, several hundred networks were trained and the best of these was chosen as the final model, ORFN (Ref. 13). The best network consisted of 6 hidden nodes, along with the fixed 14 input nodes and the single output node. The network architecture is shown in Fig. 1. The two square nodes in the input and hidden layers in Fig. 1 represent the bias, which corresponds to a constant in the weighted sums over all nodes in a layer. In this figure, the line types and line thicknesses schematically represent the sign and magnitude of the weights between nodes, as described in the figure caption. The actual parameters for the model are given in the appendix.

Several hurdles had to be overcome when generating the database for training and testing the neural network model. First, many welds were made with a pulsed laser, and the small size of the welds prohibited the direct measurement of FN. Consequently, a conversion routine was needed to convert volume percent ferrite to FN so all the data were consistent. Second, a simple and consistent means for calculating the cooling rate, both for 2-D and 3-D heat flow conditions, was required. Third, in order to use the large dataset that was the basis of earlier composition-only models, cooling rates had to be "assigned" to all those data. Fourth, some consistent approach was needed to address data that were missing chemical analyses for some of the elements considered in the model. Finally, new data were generated to supplement the data in the

KEY WORDS

Ferrite Number
Neural Network
Duplex Stainless Steel
Austenitic Stainless Steel
Ferrite Content
Cooling Rate
Alloy Composition
Constitution Diagram

J. M. VITEK and S. A. DAVID are with Oak Ridge National Laboratory, Oak Ridge, Tenn. C. R. HINMAN, formerly an intern at Oak Ridge, is now at Syracuse University, Syracuse, N.Y.

Paper presented at the AWS Annual Meeting, March 4–7, 2002, Chicago, Ill.

1. Ferrite Number rather than volume-percent ferrite is the preferred measure of ferrite content (Ref. 1).

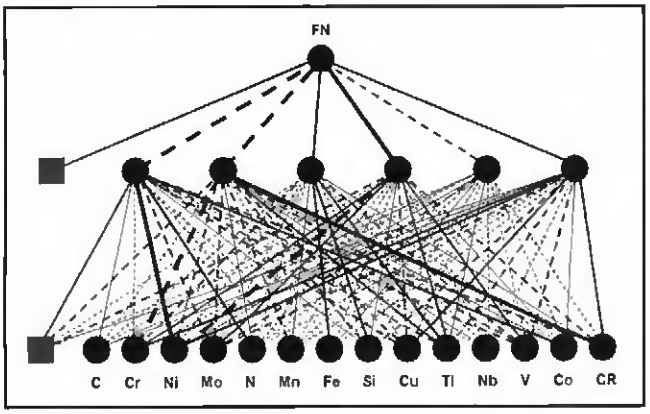

Fig. 1 — Final ORFN neural network model structure. The square nodes represent bias nodes corresponding to a constant input. Dashed lines represent negative weights between nodes while solid lines signify positive weights. Line thicknesses correspond to different ranges for the absolute values for the connecting weights: thin lines correspond to weights (absolute values) of 0 to <1.0; medium thickness lines represent weights from 1 to <4.0; thick lines correspond to weights ≥ 4.0.

literature and enhance the model with regard to its applicability to duplex stainless steels. All of these issues are described in detail in earlier publications and the reader is referred to those articles for further information (Refs. 10, 13). The final ORFN neural network model was developed on a dataset containing 1196 points. This complete dataset was comprised of three parts: the WRC dataset used to develop the WRC-1992 constitution diagram (Ref. 8) and FNN-1999 composition-only model (Refs. 10, 11); the "DVH" dataset that consists of data from an earlier investigation into cooling rate effects in stainless steel welds (Ref. 14); and the "NEW" dataset with data generated in this study (Ref. 13). The ranges of variables (composition, cooling rate) included in the complete training dataset are listed in Table 1.

Results

The predicted FN values for the entire dataset of 1196 points are plotted against the experimental values in Fig. 2A. For such a plot, the degree to which the predicted values agree with the experimental values is an indication of the accuracy with which the data are fitted in the model since the data were used to train the neural network.

Comparison of New ORFN Model with Other Models

The results from the new cooling-rate-inclusive neural network model (ORFN) can be compared with predictions of other models to see how well the models fit the experimental data. In Fig. 2B, the predicted FN using the FNN-1999 model are plotted against the experimental values, and a similar plot is presented in Fig. 2C for predictions using the WRC-1992 model. These plots include the data generated under higher cooling rate conditions and the superiority of the new model is unmistakable. Both the FNN-1999 and the WRC-1992 models (Fig. 2B and C) show significant errors. Although the new ORFN model was trained on the entire dataset, including the DVH and NEW datasets, and therefore some improvement in the overall fit is expected, the primary reason for the significantly better performance of the ORFN model is based on the fact the new model allows for a cooling rate contribution to the determination of the FN, while this is totally absent in the other two models. Thus, the

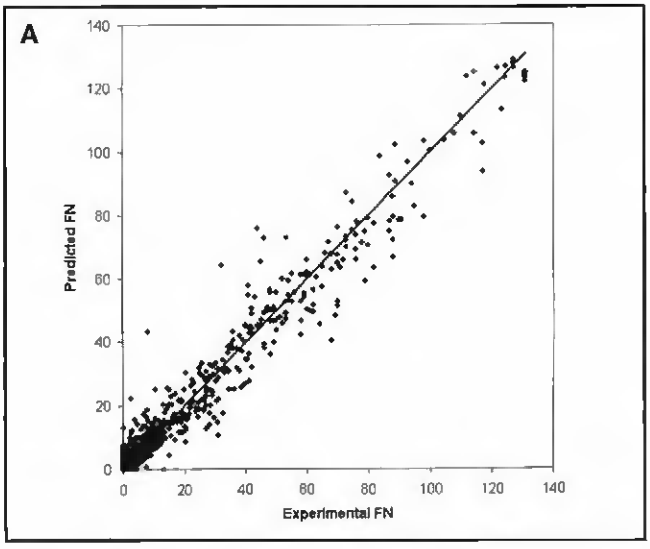

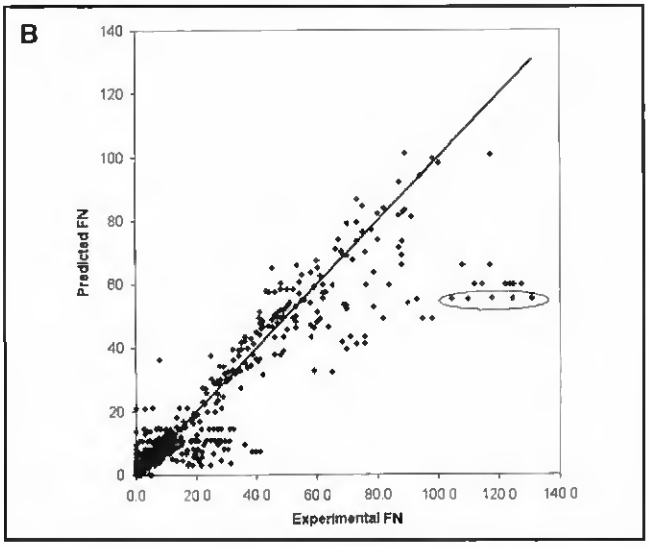

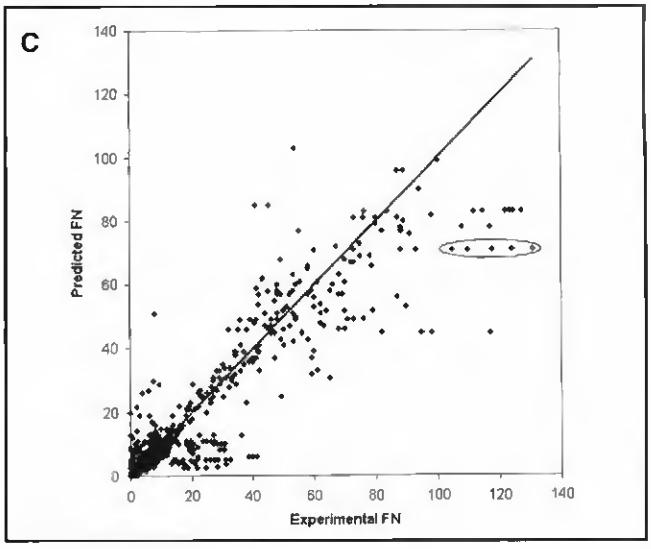

Fig. 2 — Plot of experimental vs. predicted FN using the entire training dataset (WRC + DVH + NEW) for three different models: A — ORFN; B — FNN-1999; and C — WRC-1992.

Table 1 — Composition and Cooling Rate Ranges in Dataset Used for Training ORFN

Input data		min.	max
Concentration (wt-%)	Fe	45.60	72.52
	Cr	14.74	32
	Ni	4.61	33.5
	C	0.008	0.2
	N	0.01	0.33
	Mo	0.01	6.85
	Mn	0.35	12.67
	Si	0.03	1.3
	Cu	0.0	3.04
	Ti	0.0	0.54
	Nb	0.0	0.88
	V	0.0	0.23
	Co	0.0	0.45
	Log Cooling Rate (°C/s)	1.00	6.54

Table 2 — Comparison of RMS Errors for Three FN Prediction Models (Smaller RMS Represents Better Fit to Data)

Model	RMS using entire dataset, with high cooling rate data (1196 points)	RMS using WRC dataset only (961 points)
ORFN	4.70	3.88
FNN-1999	11.00	3.52
WRC-1992	9.92	5.84

Table 3 — Compositions of Alloys Evaluated in Fig. 3 (wt-%)

Alloy	Fe	Cr	Ni	C	N	Mo	Mn	Si	Cu	Ti	Nb	V	Co
304B	70.258	18.29	8.7	0.066	0.018	0.15	1.31	0.74	0.15	0[a]	0.01	0.05	0.22
312B	59.09	29.72	8.78	0.11	0.01[a]	0.2	1.68	0.39	0[a]	0[a]	0[a]	0[a]	0[a]
316A	66.488	17.01	11.44	0.04	0.022	2.3	1.95	0.3	0.19	0[a]	0.01	0.04	0.17

(a) Value assigned in neural network analysis since chemical analysis was not available.

ORFN model can predict different FN values for the same alloy composition when the weld conditions are changed, whereas the other models predict only one FN for a given alloy regardless of the weld conditions and corresponding cooling rate. This effect of cooling rate is readily demonstrated. Consider, for example, the data within the circled regions in Fig. 2B and C. These data were generated for the same alloy composition and, consequently, the two earlier models predict the same FN for all conditions, even though the measurements show an unmistakable and substantial variation due to different weld conditions and cooling rates. In contrast, the new ORFN model takes the cooling rate into account and predicts different FNs for the same alloy when the cooling rates are different. As shown in Fig. 2A, the new neural network model fits the data quite well, covering a wide range of cooling rates (10 to $> 3 \times 10^6$ °C/s) and FN (0 to 131) (Table 1). A quantitative comparison can be made with the use of the root mean square (RMS) error values[2], which are listed in Table 2 (discussion of the RMS values for the WRC-only dataset, also listed in Table 2, is in a later section). The errors for the ORFN model are considerably lower than those for either the FNN-1999 or the WRC-1992 models when the high cooling rate data are included; a drop in RMS of more than 50% is found. The somewhat lower RMS for the WRC-1992 model compared to FNN-1999 is meaningless because both RMS values are unacceptably high.

The differences in predictions using the three models (ORFN, FNN-1999, and WRC-1992) are examined in greater detail in Fig. 3. The figure shows the predicted FN versus cooling rate for three of the alloys used to generate the NEW dataset (Ref. 13): 304B (Fig. 3A), 316A (Fig. 3B), and 312B (Fig. 3C). The alloy compositions are listed in Table 3. These alloys were chosen because they were among the few alloys for which experimental data covering a large range in cooling rate were available. The experimental measurements are superimposed on the figures. The experimental data show a strong variation in FN with cooling rate, and only the new ORFN model has the ability to describe this behavior since the other models are independent of cooling rate. It can be seen the ORFN model fits the experimental data reasonably well. This is true for both the austenitic stainless steel alloys such as 304 and 316, where the FN increases and then decreases with cooling rate, and the duplex stainless steel alloy 312, where the FN increases monotonically with cooling rate until a maximum FN corresponding to 100% ferrite is reached. It is also worth noting all three models predict nearly the same FN at the lowest cooling rate, especially for Alloys 304 and 316. This is an indication all three models do a reasonable job fitting the data for low cooling rate conditions.

A fair amount of scatter is evident in the experimental data plotted in Fig. 3 and in data for other alloys as well. There are two primary sources for this scatter: the cooling rate calculations are of limited accuracy, and the experimental measurements may be in error. In most cases, the different cooling rates correspond to systematic changes in welding speed or laser power. Therefore, the absolute cooling rates may not be accurate but the sequence of the data points in terms of increasing cooling rate is likely to be correct. Nevertheless, some irregularities may exist when cooling conditions changed from a 2-D condition at high heat input to a 3-D condition at low heat input. The larger instances of scatter and erratic data behavior are more likely due to inaccuracy of the FN measurements themselves. For high cooling rate welds, the measurements were made by metallographic identification of volume-percent ferrite and potential sources of error in this technique are well documented. Furthermore, the conversion from volume-percent ferrite to FN has some uncertainty as well. Given that the data are somewhat stochastic in nature, the predicted curves seem to show a reasonably smooth variation that duplicates the overall alloy behavior. The plots in Fig. 3 indicate the new ORFN model will properly predict overall trends, but some degree of uncertainty must be accepted with the predictions.

True Predictability Assessment

The preceding plots comparing predicted FN with experimental results are an indication of how well the models fit the data on which they were trained. However,

2. $RMS = \sqrt{\sum(Experimental\ FN - Predicted\ FN)^2)/1196}$

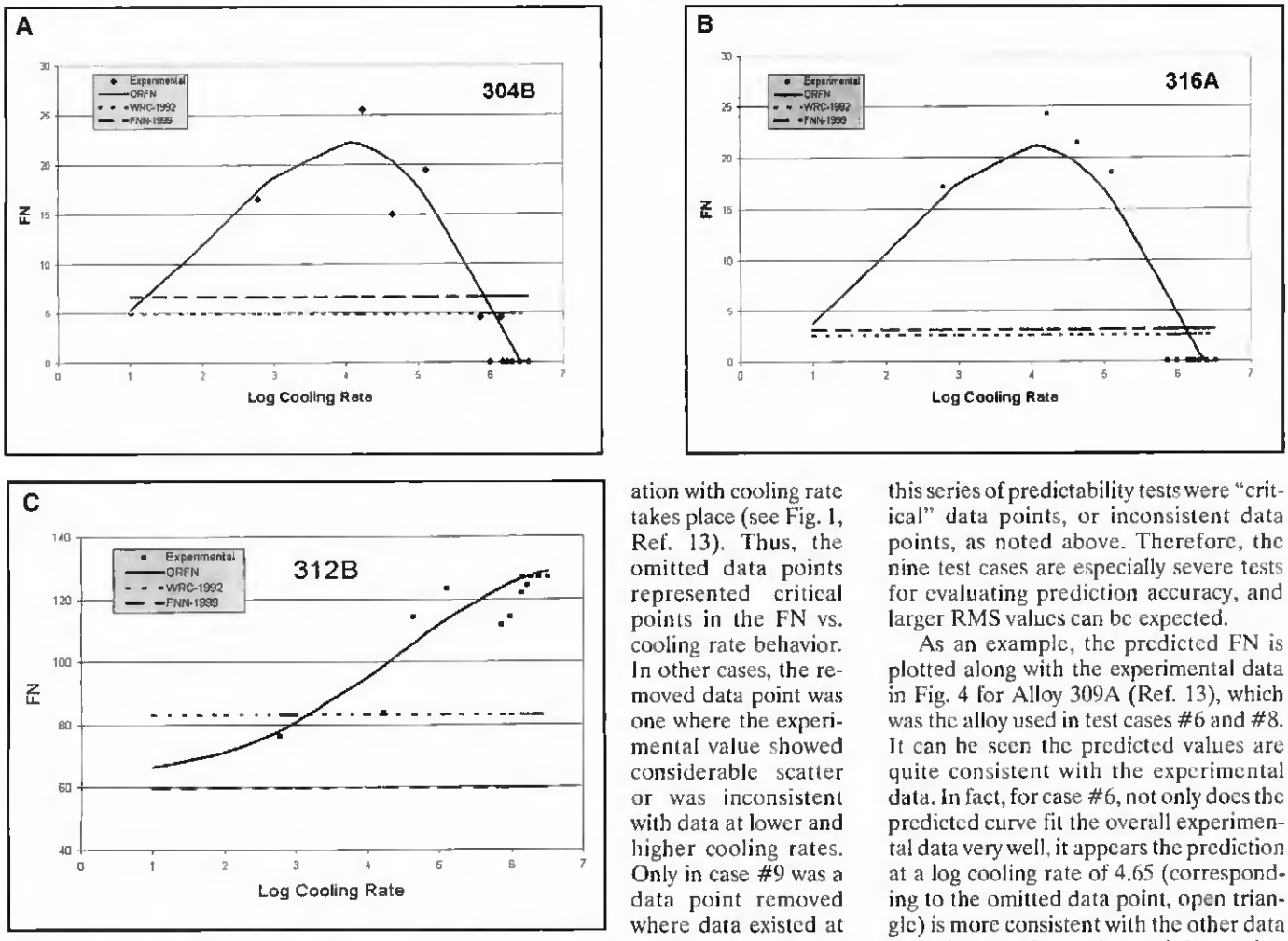

Fig. 3 — Plots showing predicted FN vs. cooling rate for three specific alloys (Table 3). Experimental data points are superimposed. Predictions for three models (ORFN, FNN-1999, WRC-1992) are shown as solid lines. A — Alloy 304B (austenitic stainless steel); B — Alloy 316A (austenitic stainless steel);, and C — Alloy 312B (duplex stainless steel).

there is a need to assess the true predictability of the ORFN model. This was done as follows. Nine separate tests were conducted in which a single data point was removed from the entire training dataset and new neural networks were calculated. In each case, many networks were calculated using the same single-point-depleted datasets in order to arrive at a "best" network. As was the case for the models trained on all the data, the use of different starting weights and data sequences produced slightly different final networks and the best among these was chosen (Ref. 13). These networks were then used to predict the FN for the data point that was purposely left out. In this way, the calculated FN values are true predictions.

Before examining the results of this predictability test, some discussion of the data points that were purposely removed is appropriate. Nine different cases were examined. In many cases, the data represented values where a maximum FN is expected or where a reversal in the FN variation with cooling rate takes place (see Fig. 1, Ref. 13). Thus, the omitted data points represented critical points in the FN vs. cooling rate behavior. In other cases, the removed data point was one where the experimental value showed considerable scatter or was inconsistent with data at lower and higher cooling rates. Only in case #9 was a data point removed where data existed at cooling rates below and above the removed point and where the data were very consistent.

The prediction results are shown in Table 4, where the predicted values for the nine tests are compared with the experimental FN as well as the predictions from the three best neural networks that were trained on the entire dataset (including the data that were omitted in the prediction runs). A few points are worth noting from the listing in Table 4. First, the true "predicted" FNs are very close to the values derived from the other networks, where the data points were included in the training. Thus, the predictability of the networks is comparable to the ability of the networks to fit the data. This same conclusion was reached for the composition-only FNN-1999 model (Refs. 10, 11) and is confirmed by the comparable RMS errors determined for the group of nine predictions. It is interesting that the RMS errors in Table 4 are noticeably higher than the errors over the entire dataset (compare Tables 2 and 4). This is due to the fact the RMS errors are calculated over a small set of data and that many of the data points used in this series of predictability tests were "critical" data points, or inconsistent data points, as noted above. Therefore, the nine test cases are especially severe tests for evaluating prediction accuracy, and larger RMS values can be expected.

As an example, the predicted FN is plotted along with the experimental data in Fig. 4 for Alloy 309A (Ref. 13), which was the alloy used in test cases #6 and #8. It can be seen the predicted values are quite consistent with the experimental data. In fact, for case #6, not only does the predicted curve fit the overall experimental data very well, it appears the prediction at a log cooling rate of 4.65 (corresponding to the omitted data point, open triangle) is more consistent with the other data than the actual experimental data point. Furthermore, both predicted curves show the same trend, indicating the predicted behavior is consistent and does not vary significantly with the inclusion or exclusion of a specific data point. Thus, in spite of the relatively large differences between the measured (14.3, 7.8) and predicted (25.7, 18.4) values for cases #6 and #8, respectively, the trends identified by the neural network appear to be correct. Data scatter also was significant for cases #4 and #5, where the predictions and experimental results are not in good agreement and the discrepancy may be more of a reflection of the scatter in the experimental data rather than the inaccuracy of the neural network prediction. It is noteworthy that in all nine cases shown in Table 4, when the network predictions are quite close to the experimental values (tests 1, 2, 9), they are close for all the network models, and when the network predictions show larger errors (tests 3–8), they show larger errors for all four networks. Thus, the inclusion of the data for training did not result in improved models. This observation implies that when significant prediction errors are found, the cause may be unreliable experimental data more than inaccurate predictions.

Discussion

It was shown in the earlier, composition-only neural network model (FNN-1999) that a significant improvement in FN prediction accuracy could be achieved with the neural network compared to the traditional constitution diagram model (WRC-1992). It is important when expanding the predictive model to include cooling rate and, in particular, high cooling rates, the prediction accuracy for low cooling rate conditions corresponding to conventional arc welding is not sacrificed. To confirm the predictive accuracy for low cooling rates is not compromised in the ORFN model, two comparisons can be made. First, the new, cooling-rate-inclusive ORFN model can be compared to the earlier FNN-1999 and WRC-1992 models when considering only the WRC dataset (which has no high cooling rate data). Plots of predicted versus experimentally measured FN are shown in Fig. 5. It can be seen the accuracy of the ORFN model is comparable to the FNN-1999 model for this limited dataset and is considerably better than the WRC-1992 model. The comparison is quantified in Table 2. A very small increase in RMS error is found for the ORFN model compared to FNN-1999, while the improvement over the WRC-1992 model is still large (≈ 34%). In this comparison, the ability of the three models to fit the data is assessed and it must be remembered that the FNN-1999 and WRC-1992 models were trained on this dataset alone, whereas the ORFN model was trained on a 25% larger dataset covering many different alloys and cooling rates.

A second, more severe test of the models can be made by comparing predicted vs. experimental FN values for a totally independent dataset. Such a dataset was compiled by Ornig (Ref. 15) and was used in other studies as a test dataset (Refs. 11, 16). It is referred to as the supplemental dataset and is described in greater detail in Ref. 11. It consists of 265 points produced under conventional (low cooling rate) conditions by arc welding. It also has a more restricted range of compositions than the entire training dataset, as noted in Ref. 11. Plots of predicted versus measured FN are shown in Fig. 6 for all three models, and corresponding RMS values are listed in Table 5. In this case, the ORFN model shows a smaller RMS than the other two models and the better fit is apparent in Fig. 6. Based on these comparisons, it can be concluded the predictive accuracy for low cooling rate conditions is not sacrificed in the new ORFN model, which is designed to cover a broader range of conditions.

The variation in predicted FN as a function of cooling rate shown in Fig. 3 is exactly what is expected from a theoretical viewpoint and shown schematically in Part 1 (Fig. 1, Ref. 13). The new model predicts an initial increase in FN for austenitic stainless steels with increasing cooling rate, and this corresponds to the inhibition of the solid-state ferrite-to-austenite transformation. At the highest cooling rates, the predicted FN decreases with cooling rate, in accord with the transition to a primary austenitic solidification mode. In contrast, the model predicts a monotonic increase in FN with cooling rate for duplex stainless steels, corresponding to the suppression of any transformation of ferrite upon cooling. In these steels, the primary solidification of austenite is not possible and so a reversal in behavior is not expected and the model does not predict it.

With the inclusion of data for several duplex stainless steel alloys in the NEW dataset, the applicability of the ORFN ferrite prediction model to duplex stainless steels is more reliable and accurate. This is a significant extension of the earlier FNN-1999 neural network model, even for low cooling rate conditions. Furthermore, the inclusion of cooling rate effects is especially important when considering duplex stainless steels since their microstructures are very sensitive to cooling

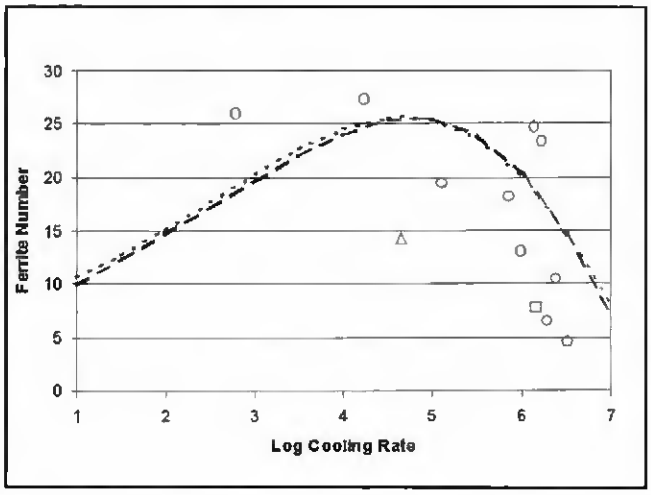

Fig. 4 — FN vs. cooling rate for Alloy 309A showing scatter in the data and the ability of the predictions to follow trends in spite of apparent large discrepancies between experiment and prediction. Data points represent experimental data. The triangle represents the experimental value for prediction case #6 and the square represents the value for prediction case #8. The short-dash line is the predicted FN vs. cooling rate for case #6 and the long-dash line is the predicted behavior for case #8.

Table 4 — Comparison of FN Values and RMS Errors for Prediction Tests (Network Trained on All but One Data Point) and Three Best Networks (Networks Trained on All Data Points)

Test Number	Experimental FN	Predicted FN	FN from Best Network (ORFN)	FN from 2nd Best Network	FN from 3rd Best Network
1	70	66.8	67.6	66.4	67.9
2	59	58.1	55.5	54.6	55.9
3	90	74	78.4	71.5	70.9
4	38.4	22.5	25.8	25.5	24.6
5	31.1	6.4	10.7	10.7	9.3
6	14.3	25.7	25.5	23.7	25.9
7	28.2	21	17.8	16	17.5
8	7.8	18.4	18.8	18.6	20.5
9	124.2	123.8	123.4	125.3	124.2
RMS error		12.6	11.0	12.1	12.7

Table 5 — Comparison of RMS Errors on the Supplemental Dataset for Three FN Prediction Models (Smaller RMS Represents Better Fit to Data)

Model	RMS using supplemental dataset, with no variation in cooling rate (265 points)
ORFN	1.84
FNN-1999	2.24
WRC-1992	2.59

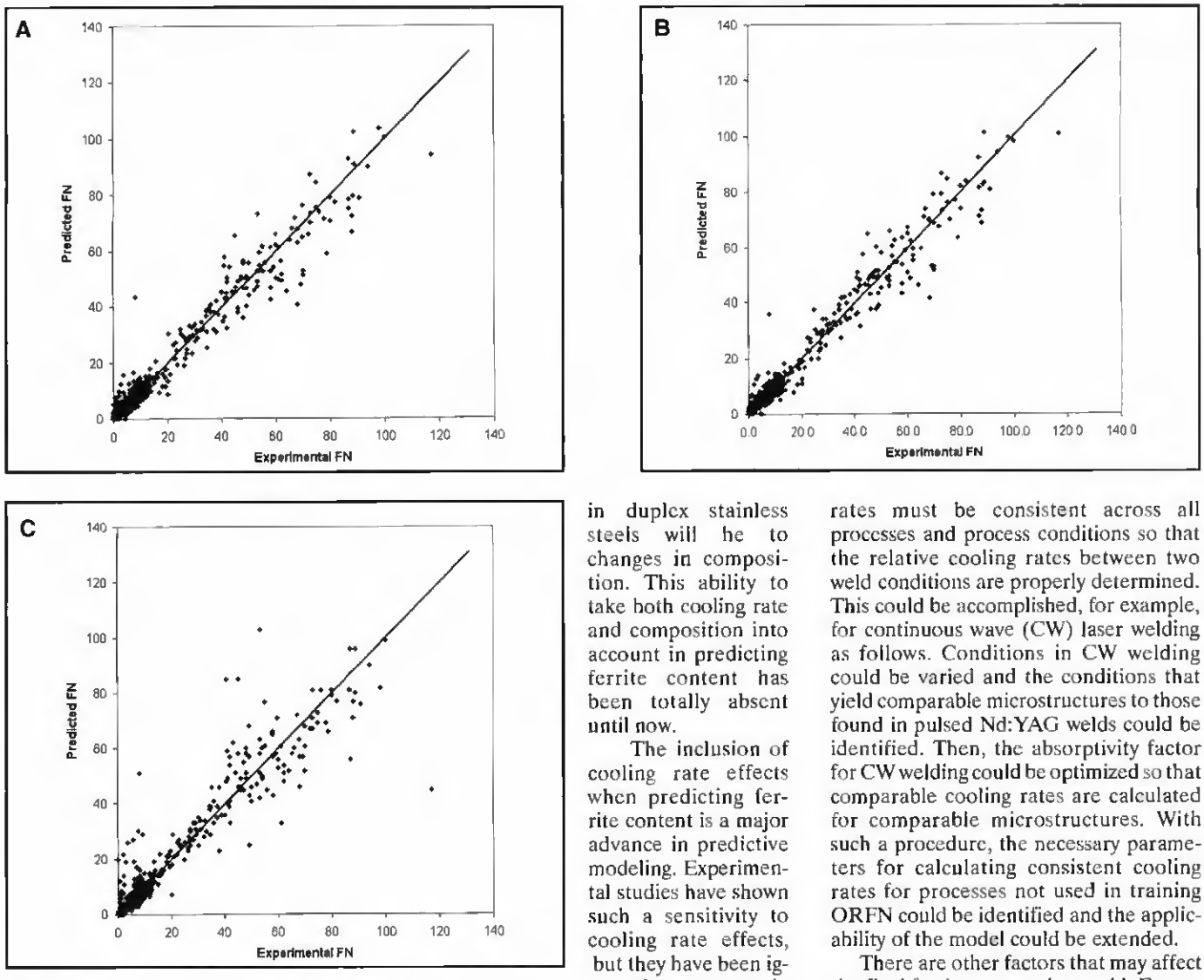

Fig. 5 — Plot of experimental vs. predicted FN for the WRC dataset (no high cooling rate data) for three different models: A — ORFN, B — FNN-1999, and C — WRC-1992.

rates. Although these steels do not exhibit any change in solidification mode when welded under high cooling rate conditions, the austenite formation during cooling after solidification can be readily suppressed. Thus, even at modest cooling rates, they may contain widely different levels of austenite, and, consequently, their properties at room temperature may vary considerably. Such effects are taken into account by the ORFN model.

The ORFN model can also be used to predict the propensity of an alloy to change solidification mode. The critical cooling rate for a given alloy can be easily calculated. In addition, the effect of changes in composition on the tendency to change solidification mode can be readily determined. Similarly, the model can determine how sensitive the ferrite content in duplex stainless steels will he to changes in composition. This ability to take both cooling rate and composition into account in predicting ferrite content has been totally absent until now.

The inclusion of cooling rate effects when predicting ferrite content is a major advance in predictive modeling. Experimental studies have shown such a sensitivity to cooling rate effects, but they have been ignored up to now in predictive models. Thus, the ORFN model is a much more robust tool for welding and weld microstructure prediction. Limited example calculations and information on obtaining the model can be found at our Web site: *engm01.ms.ornl.gov*. All of the parameters needed to calculate the predicted FN are given in the appendix. The recommended composition range for the model is the same as the composition range for the training data set given in Table 1.

There are, however, several areas in which improvements to the model can be made. The cooling rate calculations can be improved so that variations in material properties are taken into account. In addition, the extension to other welding processes, such as continuous wave laser welding, CO_2 laser welding, or electron beam welding, must be investigated. The critical issue is that the calculated cooling rates must be consistent across all processes and process conditions so that the relative cooling rates between two weld conditions are properly determined. This could be accomplished, for example, for continuous wave (CW) laser welding as follows. Conditions in CW welding could be varied and the conditions that yield comparable microstructures to those found in pulsed Nd:YAG welds could be identified. Then, the absorptivity factor for CW welding could be optimized so that comparable cooling rates are calculated for comparable microstructures. With such a procedure, the necessary parameters for calculating consistent cooling rates for processes not used in training ORFN could be identified and the applicability of the model could be extended.

There are other factors that may affect the final ferrite content in a weld. For example, minor alloying additions may alter the fluid flow conditions within the weld, resulting in a significant change in weld pool shape and corresponding weld cooling rate. It is unlikely any model can accurately take all such factors into account. Therefore, under the best of conditions, a predictive model must be considered as an estimator with limited accuracy.

Recent advances in heat and fluid flow modeling, solidification modeling, and kinetics modeling suggest that in the future one may be able to model the entire transformation behavior directly. Up to now, however, such models are of limited accuracy. For example, kinetic modeling of the solidification and ferrite-to-austenite transformation during cooling consistently overpredict the final ferrite content (Refs. 17–19). Improvements in such models are to be expected in the future. Thus, it is possible theoretical models will be able to predict behavior more accurately without resorting to empirical methods. However, such modeling re-

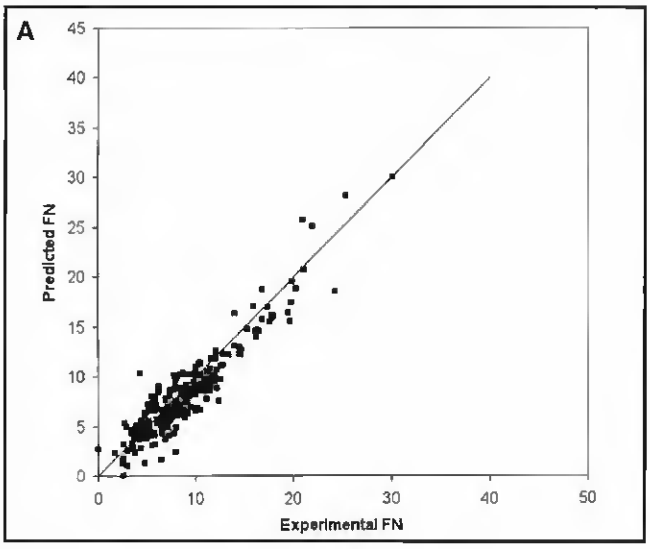

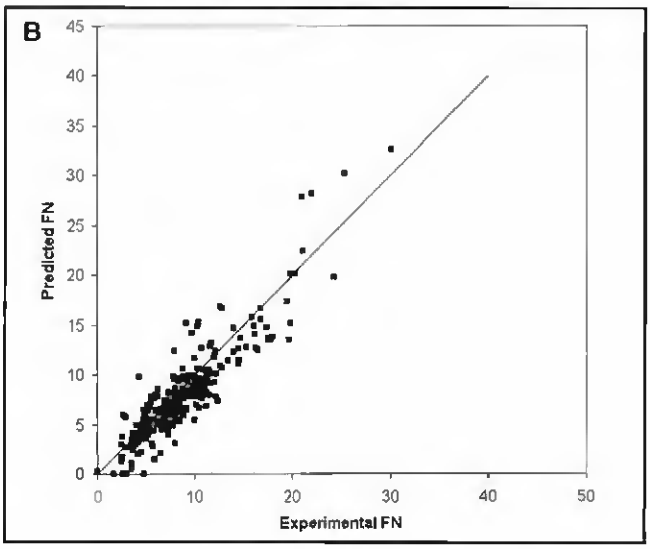

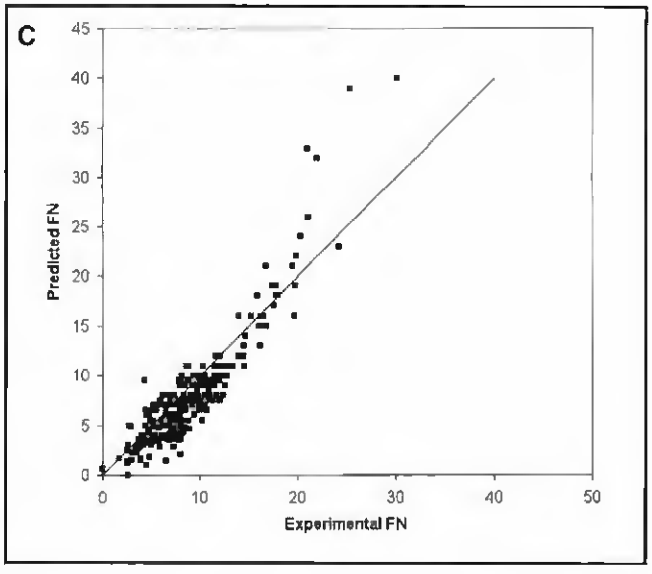

Fig. 6 — Plot of experimental vs. predicted FN using the supplemental dataset (that was not used in the training of any of the models) for three different models: A — ORFN; B — FNN-1999, and C — WRC-1992.

quires intensive computation, especially if it is extended to cover a wide range of compositions and is combined with computationally intensive heat and fluid flow models. When all of these models are developed to the point where they are accurate and reliable, they may be ideal for use in generating data for training a more user-friendly and computationally less demanding neural network model. Such artificial data would also eliminate the uncertainty and error in experimental data due to FN measurement, chemical analysis, etc. Under such conditions, gaps in the training database due to limited experimental data or difficult experimental conditions can be eliminated and the resultant model should be significantly more accurate.

Summary and Conclusions

A neural network model has been developed for predicting Ferrite Number (FN) in stainless steels welds as a function of cooling rate and composition. This new model, called ORFN (Oak Ridge Ferrite Number), allows, for the first time, the prediction of FN as a function of composition and weld process conditions (weld speed, welding power, material thickness) for both conventional arc welding and more rapid cooling rate processes such as laser beam welding. The significant effects of cooling rate on final ferrite content have been well documented and this new model takes these effects into account. It is shown that the extension of the neural network analysis to include cooling rate has not sacrificed the accuracy of the earlier, composition-only model for low cooling rate conditions. The new ORFN model takes account of changes in ferrite content due to suppression of the solid-state ferrite-to-austenite transformation, as well as changes in the primary solidification mode that are found in austenitic stainless steels at high cooling rates. The accuracy of the model was tested by various means and the results showed the present ORFN model is far superior to any other predictive model. In the development of the model, several assumptions and simplifications had to be made. These are described and possible avenues for further research and improvements to the model have been identified.

Acknowledgments

The authors would like to thank Y. Iskander for help with the neural network development in the early stages of this program. R. Reed, Oak Ridge National Laboratory, is thanked for preparing many of the welds in this study. The authors would like to thank the following people for providing materials for generating new data: D. Kotecki, The Lincoln Electric Co., Cleveland, Ohio; F. Lake, ESAB Welding and Cutting Products, Hanover, Pa.; S. Jana, Hobart Brothers, Troy, Ohio; and R. Gower, Carpenter Technology Corp., Reading, Pa. The authors would like to acknowledge the ERULF program of the U.S. Department of Energy, administered by Oak Ridge Associated Universities, Oak Ridge, Tenn., for providing the means for one of the authors (C.R.H.) to participate in this research. This research was sponsored by the Division of Materials Sciences and Engineering, U.S. Department of Energy, and the Office of Science, Laboratory Technology Research Program, U.S. Department of Energy, under contract DE-AC05-00OR22725 with UT-Battelle, LLC.

References

1. Kotecki, D. J. 1997. Ferrite determination in stainless steel welds – advances since 1974. *Welding Journal* 76(1): 24-s to 37-s.

2. Schaeffler, A. 1949. Constitution diagram for stainless steel weld metal. *Metal Progress* 56: 680–680B.

3. Hull, F. C. 1973. Delta ferrite and martensite formation in stainless steels. *Welding Journal* 52(5): 193-s to 203-s.

4. DeLong, W. T. 1974. Ferrite in austenitic stainless steel weld metal. *Welding Journal* 53: 273-s to 286-s.

5. Kakhovskii, N. I., Lipodaev, V. N., and Fadeeva, G. V. 1985. The arc welding of stable austenitic corrosion-resisting steels and alloys. *Avt. Svarka* 5: 55–57.

6. Olson, D. L. 1985. Prediction of austenitic weld metal microstructure and properties. *Welding Journal* 64(10): 281-s to 295-s.

7. Siewert, T. A., McCowan, C. N., and Olson, D. L. 1988. Ferrite Number prediction to 100 FN in stainless steel weld metal. *Welding Journal* 67(12): 289-s to 298-s.

8. Kotecki, D. J., and Siewert, T. A. 1992. WRC-1992 constitution diagram for stainless steel weld metals: a modification of the WRC-1988 diagram. *Welding Journal* 71: 171-s to 178-s.

9. Babu, S. S., Vitek, J. M., Iskander, Y. S., and David, S. A. 1997. New model for prediction of ferrite number of stainless steel welds. *Science and Technology of Welding and Joining* 2(6): 279–285.

10. Vitek, J. M., Iskander, Y. S., and Oblow, E. M. 2000. Improved ferrite number prediction in stainless steel arc welds using artificial neural networks — Part 1: neural network development. *Welding Journal* 79(2): 33-s to 40-s.

11. Vitek, J. M., Iskander, Y. S., and Oblow, E. M. 2000. Improved ferrite number prediction in stainless steel arc welds using artificial neural networks — Part 2: neural network results. *Welding Journal* 79(2): 41-s to 50-s.

12. Vasudevan, M., Murugananth, M., and Bhaduri, A. K. 2002. Application of Bayesian neural network for modelling and prediction of ferrite number in austenitic stainless steel welds. 6, ed. H. Cerjak, *Mathematical Modelling of Weld Phenomena*. London, U.K.:Institute of Materials, pp. 1079–1099.

13. Vitek, J. M., David, S. A., and Hinman, C. R. 2003. Improved ferrite number prediction model that accounts for cooling rate effects — Part 1: model development. *Welding Journal* 82: 10-s to 17-s.

14. David, S. A., Vitek, J. M., and Hebble, T. L. 1987. Effect of rapid solidification on stainless steel weld metal microstructures and its implications on the Schaeffler diagram. *Welding Journal* 66: 289-s to 300-s.

15. Ornig, H. 1988. *Proceedings International Institute of Welding 41st Annual Assembly and International Conference*. Vienna, Austria.

16. Kotecki, D. J. 1988. Verification of the NBS-CSM ferrite diagram. *International Institute of Welding Document* II-C-834-88.

17. Lee, H. M., Bae, J. S., Soh, J. R., Kim, S. K., and Lee, Y. D. 1998. Diffusional solidification behavior in 304 stainless steel. *Mater. Trans.* JIM 39(6): 633–639.

18. Hillert, M. and Höglund, L. 1999. Simulation of the peritectic reaction in 304 stainless steel. *Mater. Trans.* JIM 40(6): 567–570.

19. Vitek, J. M. 2000. Unpublished research. Oak Ridge National Laboratory, Oak Ridge, Tenn.

Appendix

Parameters for the ORFN model

In a neural network, a weighted sum of the input values is transferred to the hidden layer via a transfer function, and, in a similar manner, a weighted sum of the hidden node values is transferred to the final, output layer. In addition, the inputs and outputs are normalized with a simple linear function. Thus, the entire model can be described by the weights, normalization parameters, and the transfer function. The weights and normalization parameters are given in Tables A1, A2, and A3. The specific equations that apply, as well as the transfer functions that were used, are described in detail in Ref. 10. The equations and parameters used to calculate cooling rate are given in Part 1 (Ref. 13).

Table A1 — Normalization Parameters for Input and Output Quantities for ORFN

Data		Node	Normalization Parameters min.	max
Concentration (wt-%)	C	Input #1	0.008	0.2
	Cr	Input #2	14.74	32
	Ni	Input #3	4.61	33.5
	Mo	Input #4	0.01	6.85
	N	Input #5	0.01	0.33
	Mn	Input #6	0.35	12.67
	Fe	Input #7	45.599	72.51
	Si	Input #8	0.03	1.3
	Cu	Input #9	0.0	12.16[a]
	Ti	Input #10	0.0	2.16[a]
	Nb	Input #11	0.0	3.52[a]
	V	Input #12	0.0	0.92[a]
	Co	Input #13	0.0	1.28[a]
Log Cooling Rate (°C/s)		Input #14	1.00	6.54
Ferrite Number		Output	0	130.8

(a) "Artificial" maximum used in manner described in Ref. 10.

Table A2 — ORFN Neural Network Weight Parameters from Input Layer to Hidden Layer

	Hidden Layer Node Number					
Input Node #, Variable	1	2	3	4	5	6
1, C	+0.3208	–0.1134	–0.5135	–0.3222	+0.0663	+0.1241
2, Cr	–0.4786	–4.0781	–1.9866	+2.6729	–0.5038	+1.7295
3, Ni	+6.6912	–1.8838	–0.244	–6.1962	+0.1143	+2.7736
4, Mo	–1.792	–1.7971	–0.9168	+1.6175	–2.8306	–2.3327
5, N	+1.234	+0.0401	–0.095	–0.4997	–0.6155	–0.4854
6, Mn	–0.1341	–1.0444	+0.8119	–0.8526	–0.4334	–0.8806
7, Fe	–0.7731	–0.2389	+1.2479	–0.1887	+0.3862	–0.9014
8, Si	+0.1879	–1.112	+1.5089	+0.2254	–0.6211	–2.1438
9, Cu	–1.8901	–1.8028	–0.9316	–2.028	–0.8074	+2.0734
10, Ti	–1.827	+3.2775	+0.9634	+3.4904	+0.1944	–1.0833
11, Nb	–0.3184	+0.8096	–0.0322	–0.2077	–0.793	+0.0176
12, V	–2.0183	–1.3638	–1.1225	+3.2879	–0.2907	–3.3708
13, Co	+1.3447	+0.1086	–0.29	+0.4406	–0.1279	+0.4791
14, Log $\dot{T}$	–3.0779	+4.4439	+0.19	–1.0471	–0.5851	+1.2418
Bias	+2.5039	–2.0016	–0.3467	–1.9938	–0.1546	+0.9367

Table A3 — ORFN Neural Network Weight Parameters from Hidden Layer to Output Layer

	Hidden Layer Node Number					
Bias	1	2	3	4	5	6
+1.1759	–4.4588	–5.5929	+2.1049	+4.9924	–2.2004	+2.1616